A GROUND TO FLIGHT EXTRAPOLATION PROCEDURE FOR A LAUNCHER CONFIGURATION

A. Nicolì, B. Imperatore, M. Marini, P. Catalano
Italian Aerospace Research Center (CIRA), Capua, Italy

A.Pizzicaroli
AVIO s.p.a., Colleferro, Italy

List of symbols

Re	Reynolds based on the I stage diameter
M	Mach number
α	angle of attack
C_N	normal force coefficient
C_M	pitching moment coefficient
C_A	axial force coefficient
$C_{N\alpha}$	normal force curve slope
a	parameter of the extrapolation curves
b	slope of the extrapolation curves
k	proportionality constant
Δ	difference between two values
exp	referred to experimental condition
extr	referred to extrapolated condition
fl	referred to the flight condition

Introduction

This paper presents an experience of ground–to–flight extrapolation applied to the special case of the VEGA LV.

VEGA is a new European small launcher capable to place 300 to 2000 kg satellites, economically, into the polar and low-Earth orbits. The launcher geometry and its main parts are sketched in Fig. 1.

The VEGA external aerodynamics was experimentally and numerically characterized from M=0.5 to M=7 along the flight ascent trajectory. The wind tunnel test campaigns were performed in three World Class European wind tunnels: FOI T1500 in subsonic and transonic regime ($0.5 \leq M \leq 1.2$), DNW SST in supersonic regime ($1.6 \leq M \leq 4$) and finally DLR H2K in hypersonic regime ($5.3 \leq M \leq 7$).

The comparison between the VEGA flight trajectory and the wind tunnels envelopes (Fig. 2) shows that a maximum ratio of about 6 between the flight and the wind tunnel Reynolds numbers (evaluated using the I stage diameter as the refer-

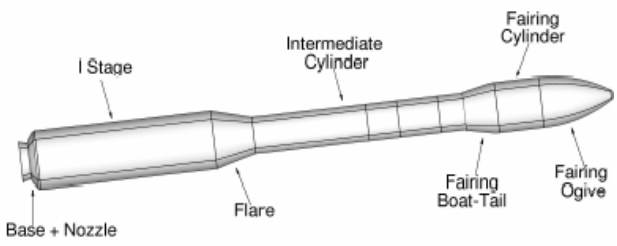

Fig. 1: Sketch of the VEGA launcher

ence length) was achieved in transonic and supersonic regime. This led to the necessity to apply an extrapolation procedure able to correct the measured aerodynamic coefficients to the flight conditions with a reasonable accuracy.

Test campaigns

Pressure measurements at several azimuth angles, global aerodynamic coefficients measurements and flow visualizations were carried out during the experimental test campaigns.

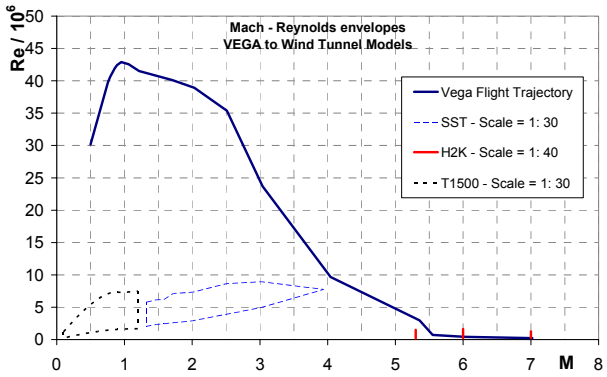

Fig. 2: Wind tunnels and flight trajectory envelopes

The model tested in subsonic, transonic and supersonic regime was scaled 1:30 with respect to the VEGA launcher. It was equipped with a six component balance; in addition, a cold jet plume simulator with an annular nozzle was installed, in order to simulate the I stage plume effect on the base pressure, and therefore on the drag. The design of the plume simulator was based on the "components method" [1]. This model was instrumented with 52 pressure taps along one model generatrix. Six additional taps were placed on the model base to form a half-ring. The surface pressures were acquired by two Electronically Scanned Pressure (ESP) transducers placed inside the model in the payload region, properly calibrated before each run.

In hypersonic regime two 1:40 scaled models where manufactured: the first one was used for global loads measurements, and equipped with a six component balance; the second one, equipped with 45 pressure taps along one model generatrix, was used for surface pressure measurements.

The pressures were acquired along 7 different azimuth positions, equally spaced of 30° between the lee- and the wind-side, in order to map the pressure field around the whole launcher. The pressure distribution was integrated in order to compute the lumped coefficients (i.e. the contribution of each launcher part, as reported in Fig. 1, to the global coefficient), which were used to improve the comparisons with the computational results.

The global aerodynamic coefficients were measured by performing angle of attack sweeps up to 10°. The aerodynamic loads were measured on both the 4 and the 3 stages configurations (the staging Mach number being about 5.6).

Up to Mach 5.3 the wind tunnels envelopes were not able to duplicate the flight conditions in terms of Reynolds number; therefore, the tests were performed at the highest pressure, i.e. Reynolds number, available. At some specific Mach numbers, as reported in Table 1, the data were acquired at more than one Reynolds number value, in order to better understand the scale effects on the aerodynamic coefficients.

Table 1

Test matrix for the force measurements

M	α	Reynolds	Configuration
0.5	0°÷10°	Max, Int., Min	Clean 4 stages
0.8	0°÷10°	Max	Clean 4 stages
0.85	0°÷10°	Max	Clean 4 stages
0.9	0°÷10°	Max, Int., Min	Clean 4 stages
0.95	0°÷10°	Max	Clean 4 stages
1.07	0°÷10°	Max, Int., Min	Clean 4 stages
1.1	0°÷10°	Max	Clean 4 stages
1.2	0°÷10°	Max	Clean 4 stages
1.58	0°÷10°	Int., Max	Clean 4 stages
1.72	0°÷10°	Max	Clean 4 stages
2.01	0°÷10°	Max, Int., Min	Clean 4 stages
3.02	0°÷10°	Max, Int., Min	Clean 4 stages
3.96	0°÷10°	Max	Clean 4 stages
5.3	0°÷10°	6 values	Clean 4 & 3 stages
6.04	0°÷10°	Flight	Clean 4 & 3 stages
7.0	0°÷10°	Flight	Clean 3 stages

Schlieren videos and pictures were taken during each run. Experimental oil flow visualizations were performed at M=0.9, 1.2, 1.58, 2.01, 3.02 and 6.04 at α=2° and/or 5°. As it will be pointed out later, the flow visualizations represented a fundamental source of information for the extrapolation process.

All subsonic, transonic and supersonic tests were performed by fixing the transition near the model nose, where it is expected at flight condition. In hypersonic regime, where the test Reynolds were close to the flight conditions, transition was left free.

Computational analysis

The CIRA RANS (Reynolds Averaged Navier Stokes equations) flow solver Z.E.N. (Zonal Euler Navier-Stokes) was applied for the numerical simulations. ZEN is a multi-block very robust, efficient and well assessed solver for the Euler and RANS equations based on a finite-volume cell-centered approach. A central differencing scheme with blended self adaptive second and fourth order artificial dissipation is employed. The solution procedure is based on a pseudo time-marching concept. The multigrid scheme is used to accelerate the convergence of the solution, and performs relaxations, by using the Runge-Kutta algorithm with local time stepping and residual averaging, on different grid levels. Several turbulence models, ranging from algebraic to high order models, are implemented and were tested on several practical applications [[2]]. The κ-ω model proposed by Kok [[3]] has been used for all the simulations presented in this paper. A time-accurate version of the code has been developed and is being validated [[4]].

Several computational grids have been generated for the full-scale configurations, and for the 1:30 and 1:40 scaled models of the launcher by means of the software package ICEM-CFD. All the meshes employ a C-O topology with external boundaries adapted to the particular flow regime. An interface, embedded in ICEM, allows to obtain a grid in a format directly readable by the CFD solver.

Numerical analyses, focused to support the extrapolation process, were performed at the conditions reported in Table 2: Reynolds number effects were evaluated at M=0.95, 3.02 and 5.3 and the experimental tests were numerically rebuilt at several Mach numbers. In the latter case, the geometry also reproduced the annular plume simulator used for the experiments [[5]].

Table 2

CFD calculations conditions

M	α	Reynolds	Configuration
0.5	2°, 5°	WT	Clean 4 stages
0.95	2°, 5°	Flight, Int., WT	Clean 4 stages
1.2	2°, 5°	WT	Clean 4 stages
2.01	2°, 5°	WT	Clean 4 stages
3.02	2°, 5°	Flight, Int., WT	Clean 4 stages
5.3	2°, 5°	Flight, WT	Clean 4 stages
6.04	2°, 5°	Flight	Clean 4 stages
6.04	2°, 5°	Flight	Clean 3 stages

Some aspects of the flow topology

A through comprehension of the flow topology around the VEGA model represented a key factor to perform the extrapolation of the aerodynamic coefficients. Hereinafter only some details of the flow topology will be presented in order to understand the extrapolation procedure adopted.

Generally, lee-side vortices structures, typical of such a kind of configuration at incidence, can be observed. In the transonic regime the flow pattern is characterized by a shock

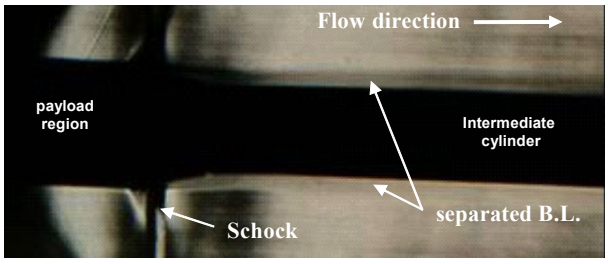

Fig. 3: Schlieren picture of the shock induced separation at M=0.95

wave–induced boundary layer separation at the boat tail at M=0.95 (Fig. 3). As the Mach number increases the shock moves towards the intermediate cylinder and a separation behind the shock is still present until it reaches the flare at about Mach 1.1. The same separation has been numerically predicted at the wind tunnel condition as well as in flight. So, the flow topology does not change within the Reynolds range of interest.

In supersonic regime the oil flow visualizations show a overall attached flow on the boat tail.

Finally, in hypersonic regime it was found that a separation occurs at low incidence at the boat tail region. This is clearly shown in the oil flow visualization pictures taken at M=6.0, on which the separation line at the boat tail at α=1° is depicted (Fig. 4). The skin friction pattern shows also that the flow does not reattach on the intermediate cylinder after the separation at the boat tail.

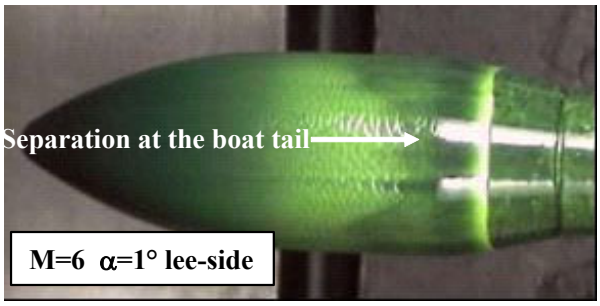

Fig. 4: Separation at the boat tail at M=6.0

The shock intensity at the flare is strongly influenced by the boundary layer thickness on the intermediate cylinder: in particular, as the Reynolds number increases, the separation on the boat tail moves forward inducing a reduction of the boundary layer thickness on the intermediate cylinder, and consequently a stronger shock wave intensity on the flare. This flow topology can explain the behavior of the aerodynamic coefficients measured in the hypersonic regime: at low incidences the axial force, plotted in Fig. 5 at M=5.3, decreases as the angle of attack increases because the flow reattaches on the lee-side; the C_A at α=0° increases as the Reynolds number increases because the intensity of the shock wave on the flare is enhanced.

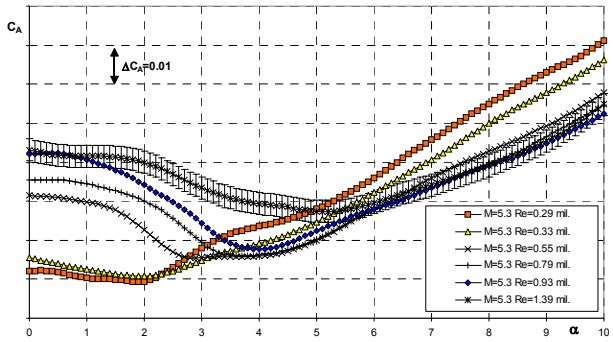

Fig. 5: Axial force coefficients at M=5.3

Extrapolation procedure for C_N and C_M

Comparison of experiments and computations

The first step in the ground to flight extrapolation procedure adopted consists in the comparison of the experimental and numerical results. The causes of the inevitable differences between the two sets of data are then identified. The necessary corrections to use all the data as a single set of information are eventually applied.

Let us consider, for example, the normal force coefficient distribution at M=3. Fig. 6 shows the comparison between the experimental and numerical trends with Reynolds number of normal force coefficient at α=2° and 5°. Both methods predict a C_N slightly decreasing as the Reynolds number increases, probably because of an upward movement of the vortices separation lines on the lee-side that induces a reduction of the vortex lift. It is worth noting that the numerical results slightly underestimate (3.8% at α=5°) the C_N with respect to the experiments. Actually, there is a systematic computational underestimation of normal force at almost all the Mach numbers

as shown in Fig. 7, where both the experimental data and the C_N computed at the same Reynolds number are plotted as function of Mach number.

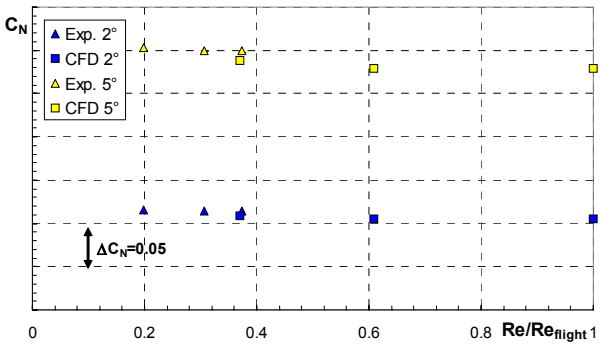

Fig. 6: Experimental and numerical C_N trends with Re at M=3

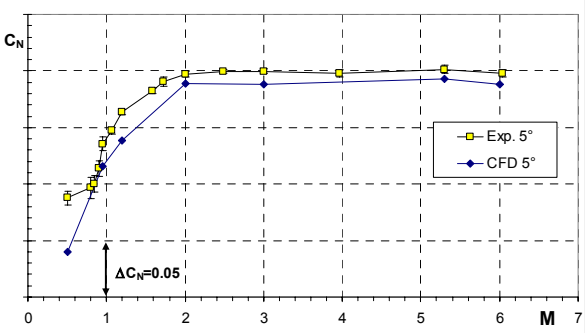

Fig. 7: Experimental and numerical C_N vs M

The lumped normal force at M=3, α=2° (Fig. 8) shows that the numerical results underestimate significantly the C_N only on the I stage, where the normal force is mainly produced as vortex lift induced by the vortices on the lee side of the model. This difference can be reasonably ascribed to a computational underestimation of the lee-side vortices strength and/or of their distance from the model surface. This is probably due to the limited grid resolution in the azimuth direction, away from the model surface, and therefore can be considered a systematic error not dependent on the Reynolds number. Based on this hypothesis the numerical results at M=3 can be corrected by shifting the data of the same amount, independently from the Reynolds number at which they are computed. The magnitude of the correction is determined as the difference between the experimental and numerical results evaluated at the higher wind tunnel Reynolds.

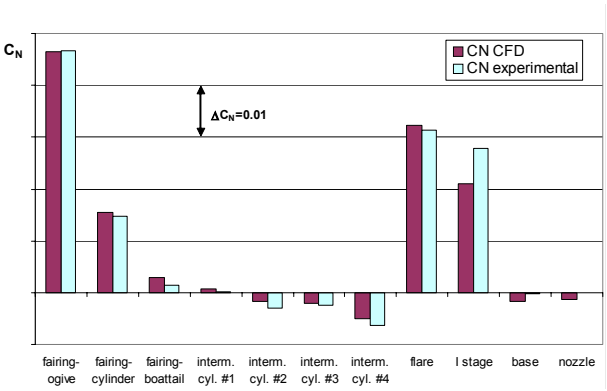

Fig. 8: Lumped C_N at M=3 α=2°

Identification of the data trends with Reynolds

Analyses like the one above have made possible to treat the two sets of data as a single one. A unique trend with Reynolds at both angles of attack at which numerical data where computed (α=2° and α=5°) was identified. This is shown in Fig. 9 where both the experimental and the corrected numerical trends with Reynolds number of the normal force coefficient at α=5° are plotted at different Mach numbers; the experimental data are reported with the error bars.

It should be noted the good agreement between the experimental and numerical trends. This is due to the fact that the same flow structures observed at the wind tunnel condition can be expected in flight. In fact, even in the most critical situation, like at M=0.95 where there is a strong viscous/inviscid interaction at the boat tail at wind tunnel conditions, the same interaction was numerically predicted at flight condition.

At each Mach number, the trends can be described by the following function:

$$C_N = a\left[Log_{10}(\mathrm{Re})\right]^{b(M,\alpha)} \quad (1)$$

represented by the continuous lines in Fig. 9.

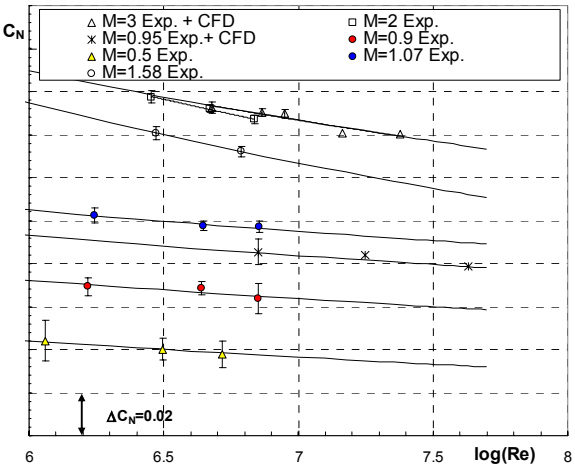

Fig. 9: C_N trends with Reynolds

This function has two advantages: first, it fits the data with a very good approximation, well within the experimental error bars; second, it has a simple form, in which the parameter b that describes the slope of the extrapolation curves can be expressed as function of Mach and of the angle of attack.

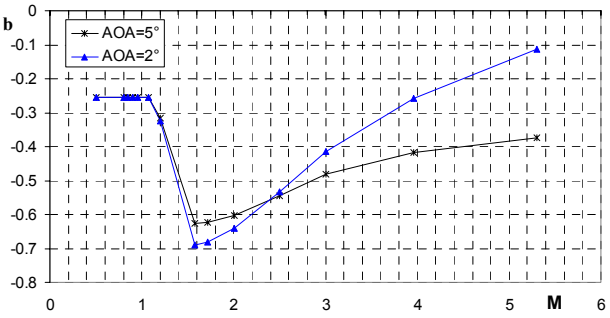

Fig. 10: The parameter b vs M

The parameter *b* as obtained from Fig. 9 is plotted as function of Mach in Fig. 10. It can be noted that in transonic regime the Reynolds effect is almost independent from the Mach number, whereas in supersonic regime, between M=1.5 and 4, it decreases as Mach increases, as expected.

Dependency on the angle of attack

The numerical trends with Reynolds number can support the extrapolation of the aerodynamic coefficients only at α=2° and α=5° where the computations are available. However, it can be observed that only $C_{N\alpha}$ is affected by changes in Reynolds number; in fact, the difference between the normal force coefficients measured respectively at the minimum and maximum wind tunnel Reynolds (Eq. 2) can be considered with a good approximation a linear function of the angle of attack (see Fig. 11):

$$\Delta C_{N_{\exp}} = C_{N_{\exp}}(\mathrm{Re}_{\min}) - C_{N_{\exp}}(\mathrm{Re}_{\max}) = k\alpha \quad (2)$$

It has to be noted that ΔC_N is very small, therefore any non linearity of this difference is negligible if compared with the experimental accuracy.

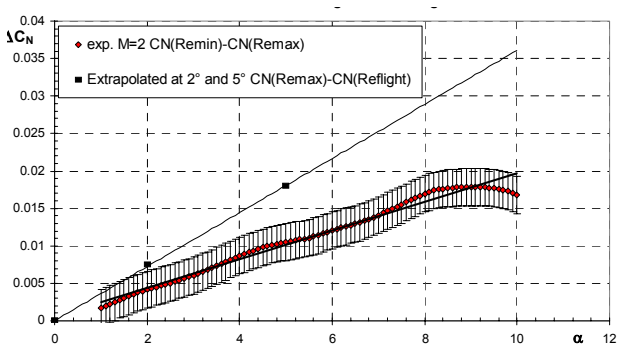

Fig. 11: Re effects on normal force at M=2

On the basis of the above considerations it is possible to model as linear the function:

$$\Delta C_{N_{fl}} = C_{N_{\exp}}(\mathrm{Re}_{\max}) - C_{N_{extr}}(\mathrm{Re}_{fl}) = k\alpha \quad (3)$$

which represents the difference between the unknown normal force coefficient in flight and the value measured at the higher Reynolds number in wind tunnel.

It is possible to evaluate the proportionality coefficient k by using the extrapolated values of ΔC_{Nfl} already computed at α=2° and α=5° as

shown in the previous section, and the condition $\Delta C_{Nfl}(\alpha=0°)=0$. The value of k which minimizes the deviation of the function kα (the black straight line in Fig. 11) from the extrapolated values at 2° and 5° (black squares in Fig. 11) was computed at all Mach numbers, as it is shown in Fig. 11 for M=2. Note that the extrapolated values of ΔC_{Nexp} at 2° and 5° represented by the black squares are almost perfectly aligned, and this enhances the hypothesis expressed by Eq. *(3)*.

The extrapolation of the pitching moment coefficient followed the same considerations done for C_N.

Extrapolation procedure for C_A

Provided that the boundary layer is fully turbulent and the flow topology is not changing with Reynolds, as it was found in subsonic and supersonic regime, it can be expected that the scale effects, at least for the model attitudes of interest, can be mainly ascribed to a reduction of the friction drag [6].

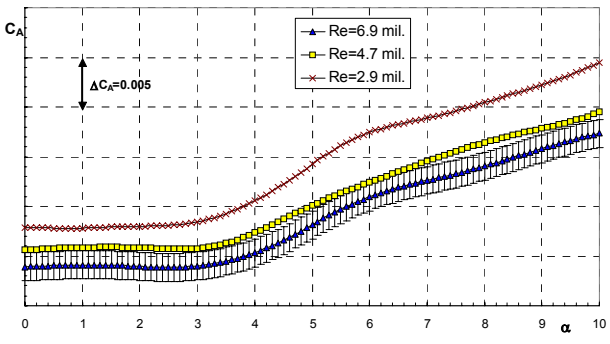

Fig. 12: Re effects on the axial force at M=2

Fig. 12, for example, shows that the Reynolds number effects at M=2 are almost independent from α. The same behavior was experimentally observed at all Mach numbers up to 4. Once more the trends with Re of this coefficient can be described with functions similar to Eq. *(1),* but in this case there is not dependency on α.

Special case: hypersonic regime

The hypothesis of considering the correction of the numerical data Reynolds number independent is not valid anymore in hypersonic regime. Let us consider for example Fig. 13, which is the analogous of Fig. 6 but at M=5.3. Again, there is an underestimation of the numerical vortex lift at α=5°, whilst at α=2° the numerical results over predict the C_N with respect to the experiments.

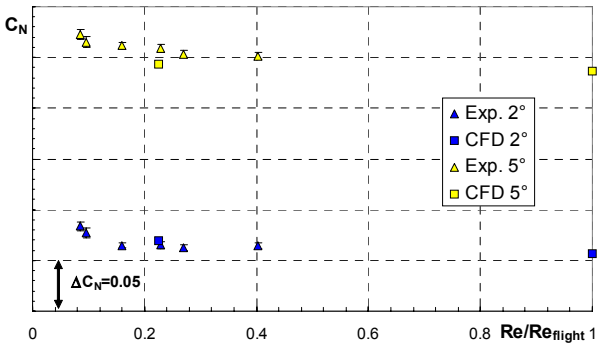

Fig. 13: C_N trends with Reynolds at M=6

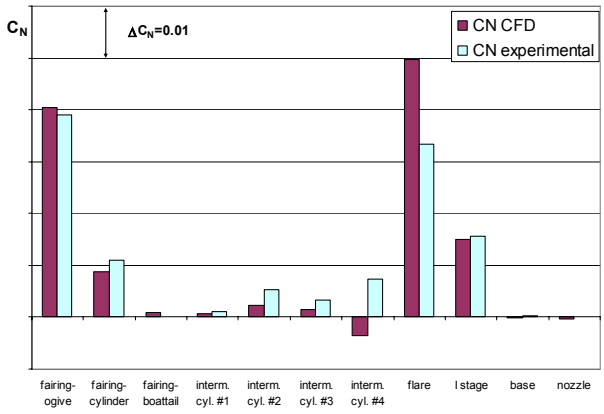

Fig. 14: Lumped C_N at M=6 α=2°

Looking at the lumped coefficients reported in Fig. 14, it can be observed that the main differences between numerical and experimental results are concentrated on the flare and on the final part of the intermediate cylinder.

The flow pattern found in the hypersonic regime suggests that, in this case, the differences between numerical and experimental

data are caused by a slightly different prediction of the separation at the boat tail, that has a downstream effect on the shock wave intensity at the flare. Finally, it can be concluded that any correction of the numerical data in this case should be strongly Reynolds number dependent in contrast with the conclusions deducted at M=3.

In addition, as already shown in Fig. 5, in the hypersonic regime the Reynolds number effects are strongly not linear with α and the hypothesis expressed in Eq. (*3*) is not valid anymore in this regime. In this case the extrapolation was performed using trends described by eq. (*1*) computed at several angles of attack (and not only at 2° and 5°) since the parameter b is not more a linear function of α. The huge number of experimental Reynolds number conditions gave a significant help to the present analyses.

Concluding remarks

The ground to flight extrapolation procedure for the aerodynamic coefficients of the VEGA launch vehicle has been presented. The extrapolation procedure is based upon the experimental and numerical evaluation of the trends with Reynolds number of the aerodynamic coefficients at several Mach numbers. CFD results were used as support to the extrapolation methodology.

It can be generally stated that a thorough knowledge of the flow structures around the vehicle, at both flight and wind tunnel conditions, and gathered by means of global aerodynamic loads and surface pressure measurements, flow visualizations and computational predictions, is absolutely necessary.

Acknowledgements

The authors wish to sincerely acknowledge the support provided by the staff of the FOI, DNW and DLR facilities, which was fundamental for making these tests successful.

References

[1] Korst H. H. White R.A., Page R.H., *Interference-free wind tunnel testing of jet propelled missiles*. Aerospace Science and Technology, vol. 2, no. 8, pp. 481-488(8), December 1998

[2] Catalano P., Amato M. An evaluation of RANS turbulence modelling for aerodynamic applications. Aerospace Science and Technology Journ., Vol. 7, pp. 493-509, 2003

[3] Kok J. C. Resolving the dependence on free stream values for the κ-ω turbulence model. AIAA Journ., Vol. 38, pp. 1292-1295, 2000

[4] Marongiu C., Catalano P., Amato M., and Iaccarino G. *U-ZEN A computational tool solving U-RANS equations for industrial unsteady applications.* AIAA paper 2004-2345, 34th AIAA Fluid Dynamics Conference, Portland (OR), June 28th – July 1st 2004

[5] Catalano P., Marini M., Nicolì A. Pizzicaroli A., *RANS simulations of a flow past a Launcher Configuration in Motor-On Condition.* 23rd AIAA Applied Aerodynamics Conference, Toronto (CA) June 6-9 2005, AIAA paper 2005-4964

[6] *Boundary Layer Simulation and Control In wind Tunnels.* AGARD AR-224, April 1988